ChemComm

COMMUNICATION

View Article Online
View Journal | View Issue



Cite this: *Chem. Commun.*, 2015, **51**, 7195

Received 14th January 2015,
Accepted 20th March 2015

DOI: 10.1039/c5cc00353a

www.rsc.org/chemcomm

# The facile synthesis of single crystalline palladium arrow-headed tripods and their application in formic acid electro-oxidation†

Na Su, Xueying Chen,* Yuanhang Ren, Bin Yue, Han Wang, Wenbin Cai and Heyong He*

**Single crystalline palladium arrow-headed tripods prepared *via* a simple one-pot strategy exhibit high electro-activity in formic acid oxidation, which could be a promising anodic catalyst for direct formic acid fuel cells.**

It is well known that the catalytic properties of the noble metal catalysts strongly depend on their shapes and the arrangement of atoms at different facets on the surface.[1–4] Thus, one promising route to develop high-performance metal catalysts is to induce the exposure of specific catalytically active facets of nanocrystals through shape-controlled syntheses. As compared to those with convex surfaces, noble-metal nanocrystals with concave surfaces have been demonstrated with enhanced catalytic properties because of their higher density of atomic steps and kinks.[5] Among them, multipod nanocrystals with branched arms naturally have concave regions on the surface and thus have received particular interest.[6–12]

Palladium plays a crucial role in many catalytic applications.[13] In electrochemical reactions, Pd appears to be of specific interest. Recently, it was reported that Pd exhibited an electro-activity, and the tolerance against CO poisoning superior to Pt in terms of formic acid electro-oxidation in direct formic acid fuel cell (DFAFC) applications,[14] which is a promising power source for portable electronic devices. Thus, the synthesis of novel Pd multipod nanocrystals is highly desirable.

Herein, we report the synthesis of single crystalline Pd arrow-headed tripods *via* a simple one-pot strategy by collectively manipulating the reduction kinetics, concentration gradient and surface diffusion of atoms. The typical preparation of the Pd arrow-headed tripods is as follows: 0.160 g of polyvinylpyrrolidone (PVP, $M_w$ = 55 000) and 0.050 g of Pd(acac)$_2$ were dissolved in 10 mL of benzyl alcohol in an $N_2$ flow at 273 K. Then, 40 μL of benzaldehyde was added to the above reaction mixture. The resulting homogeneous yellow solution was kept in an $N_2$ flow at 343 K for 6 h without stirring. The resulting products were collected *via* centrifugation and washed with ethanol and acetone to remove the excessive PVP. The final products were kept in ethanol for characterization and activity tests. Electrochemical measurements were performed using a standard three-electrode electrochemical cell and a CHI605B electrochemical working station in a 0.5 M $H_2SO_4$ + 0.5 M HCOOH solution (details are described in the ESI†). Electrochemical cleaning of the Pd arrow-headed tripods was performed by applying repetitive potential cycling between 0 and 1.0 V (*vs.* RHE) at 0.5 V s$^{-1}$ in 0.5 M NaOH following the procedures reported in ref. 15.

The images of high-resolution scanning electron microscopy (HRSEM) (Fig. 1a–c) and scanning transmission electron microscopy (STEM) (Fig. 1d) show that the dominant products are planar tripods. Some unripe tripods, such as monopods and bipods were also observed. The three arms of the tripods are 120° angles apart and the edges of the arms are composed by kinks. Moreover, the tips of the tripods are interestingly in the form of arrow-heads with the shape of a well-resolved truncated tetrahedron or an unripe concave tetrahedron. Based on the HRSEM and STEM images, together with the following SAED and HRTEM studies, the ideal structure model of Pd arrow-headed tripods is shown in Fig. 1e. Energy dispersive X-ray emission analysis (EDX) results indicated that the nanocrystals were totally composed of palladium.

The wide angle XRD pattern of the Pd arrow-headed tripods is shown in Fig. 2. For comparison, the standard pattern of the Pd black sample obtained from JCPDS (Card No. 89-4897) is also shown. There are five Pd diffraction peaks at 2$\theta$ of 40.0°, 46.6°, 68.0°, 82.0° and 86.4° in the arrow-headed tripod sample, which can be indexed to the (111), (200), (220), (311) and (222) reflections of face-centered cubic (fcc) palladium, respectively. The lattice constant of the Pd tripod is 0.390 nm, which is close to that of the Pd black from JCPDS (0.389 nm). The intensity

*Department of Chemistry and Shanghai Key Laboratory of Molecular Catalysis and Innovative Materials, Collaborative Innovation Center of Chemistry for Energy Materials, Fudan University, Shanghai 200433, P. R. China.*
*E-mail: xueyingchen@fudan.edu.cn, heyonghe@fudan.edu.cn;*
*Fax: +86 21 5566 5572; Tel: +86 21 6564 3916*

† Electronic supplementary information (ESI) available: The details of Pd electrode preparation, electrochemical measurements and CO stripping experiment, TEM images of Pd samples formed by using different Pd(II) source, TEM images of Pd samples formed with stirring, TEM images of Pd samples formed at different reaction temperatures, and cyclic voltammograms of Pd samples formed by different Pd(II) sources in a 0.5 M HCOOH + 0.5 M $H_2SO_4$ solution at a scan rate of 50 mV s$^{-1}$. See DOI: 10.1039/c5cc00353a

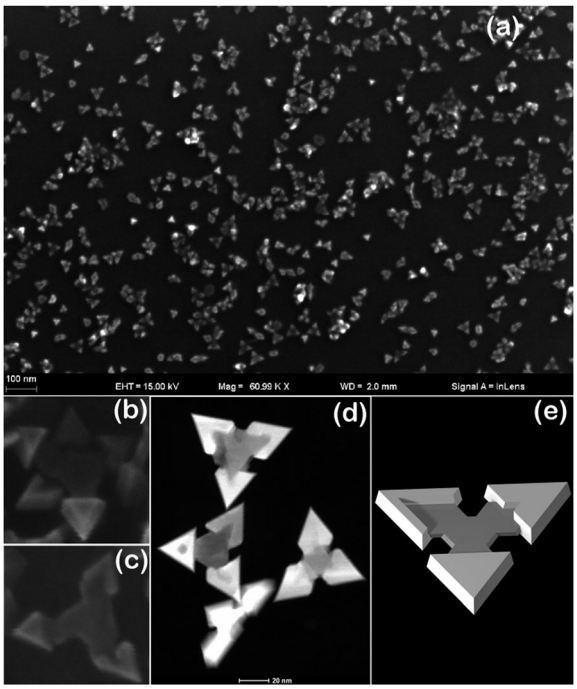


Fig. 1 HRSEM (a–c), STEM (d) images and structure model (e) of the Pd arrow-headed tripods.

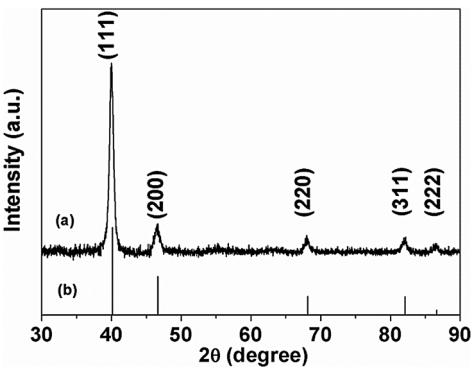


Fig. 2 XRD patterns of the Pd arrow-headed tripods (a) and Pd black sample obtained from JCPDS ((b), Card No. 89-4897).

ratio of the (111) to (200) peaks in the Pd tripod sample is thrice as that in the random Pd black sample (7.21 *versus* 2.29). As most of the tripods are easily flattened on the XRD sample holder, its (111) preferred orientation indicates that the top and bottom faces of each planar tripod are bounded by {111} planes.

According to the transmission electron microscopy (TEM) images (Fig. 3a), the average particle size of the arrow-headed tripods is in the range of 20–70 nm (tip-to-tip distance) and the width of the arm is in the range of 5–10 nm. Fig. 3b shows the typical selected area electron diffraction (SAED) pattern of an individual Pd tripod lying flat on the TEM grid (inset in Fig. 3b). The diffraction spots show a 6-fold rotational symmetry, indicating that the tripod is single crystalline and the zone axis is along the ⟨111⟩ directions of fcc palladium and the basal facets of the tripod are {111} planes.[16] The bright spots in the second circle from the

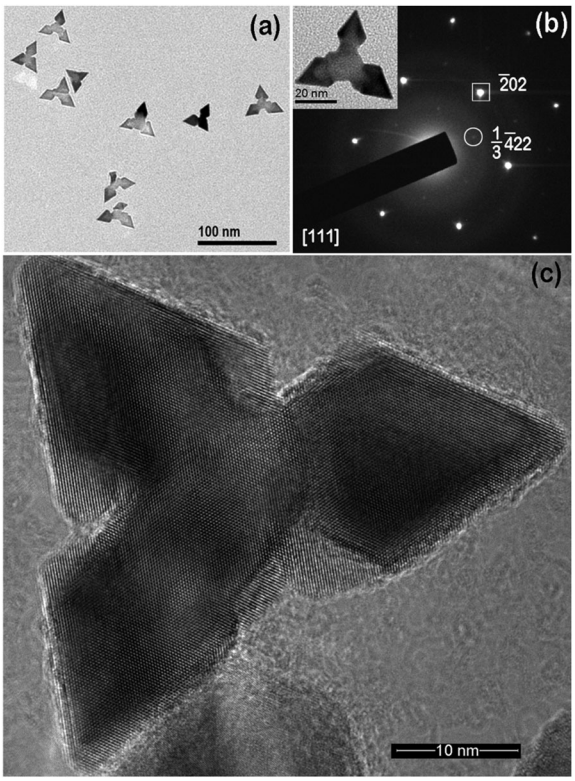


Fig. 3 TEM image (a), SAED pattern (b) and HRTEM image (c) of the Pd arrow-headed tripods.

centre with a *d*-spacing of *ca.* 1.4 Å corresponds to the {220} reflection of the fcc metallic Pd (squared spot). The calculated *d*-spacing of the inner dim spots (circled spot) is *ca.* 2.4 Å, which can be indexed as the 1/3{422} reflection of Pd. The observation of the 1/3{422} diffraction spots is usually ascribed to the presence of stacking faults in the {111} plane perpendicular to the electron beam.[16,17] Further analysis of the SAED pattern reveals that the three arms of the tripods grow along the ⟨211⟩ directions. Fig. 2c shows the HRTEM image of an individual planar tripod. Continuous lattice fringes are observed in the whole tripod, further demonstrating the single crystalline nature of the tripod.

To ensure the formation of the arrow-headed tripods, the rational control of the three most important experimental parameters, *i.e.* reduction rate, concentration gradient and reaction temperature, are found to be crucial. It was found that Pd arrow-headed tripods could only be obtained under a relatively low reduction rate by using benzaldehyde as the reductant and $Pd(acac)_2$ as the Pd(II) source. When $Na_2PdCl_4$ or $PdCl_2$ was applied in the preparation, nanodendrites or irregular Pd nanoparticles were formed (Fig. S1, ESI†). Since all the other preparation conditions were kept the same, the different Pd(II) source mainly affected the reduction rate. The faster reduction of $Na_2PdCl_4$ favoured the formation of large amounts of small Pd grains with high surface area and surface energy. Due to the presence of a large amount of PVP in the reaction mixture, the growth of the small Pd grains was slow. Large amounts of small Pd grains tended to aggregate together to lower the total surface energy and thus nanodendrites were formed.[8] In contrast, the lower reduction rate of $Pd(acac)_2$ only

 

favoured the formation of small amount of Pd grains which were difficult to be aggregated and tended to grow separately. The relatively slow growth rate probably favours the introduction of {111} stacking faults in the Pd nucleation,[18] which is essential for the formation of the planar tripods.[11] As for $PdCl_2$, although its reduction rate is similar to that of $Na_2PdCl_4$, its lower solubility in the reaction mixture makes the amount of Pd grains formed fall in between $Na_2PdCl_4$ and $Pd(acac)_2$, resulting in the formation of the products intermediate between nanodendrites and planar tripods. Besides, the introduction of concentration gradient was also found to be important for producing arrow-headed tripods. During the preparation, stirring should not be applied in order to purposely create a concentration gradient to facilitate the selective nucleation and preferential growth at the tips farthest from the centre of the planar tripods.[19] Otherwise, with stirring, the dominant products obtained are truncated tetrahedra, instead of tripods (Fig. S2, ESI†). In addition, the reaction temperature strongly affects the formation of the tripods (Fig. S3, ESI†). Relatively low reaction temperature was found to be favourable for the formation of tripods, probably owing to both the decrease of the reduction rate and the suppression of the surface diffusion of the Pd atoms to confine the growth at tips. The detailed growth mechanism of Pd arrow-headed tripods still requires further study.

Fig. 4A shows the cyclic voltammograms (CVs) of commercial Pd black (a) (BASF, average particle size of *ca.* 10 nm), and the Pd arrow-headed tripods as-prepared (b) and electrochemically cleaned[15] (c) in 0.5 M $H_2SO_4$ at 50 mV $s^{-1}$. As for the as-prepared Pd arrow-headed tripods, characteristic features of hydrogen adsorption/desorption were not observed, indicating that the surfaces of the tripods are blocked by the residual PVP. The electrochemically cleaned Pd arrow-headed tripods displayed characteristic sharp and symmetric hydrogen adsorption/desorption peaks similar to the CVs of commercial Pd black, indicating that the surfactant PVP was largely removed. Fig. 4B compares the formic acid oxidation mass activities on the above three electrode catalysts. The forward peak current for formic acid electro-oxidation on the as-prepared Pd arrow-headed tripods is 401.0 mA $mg^{-1}$ Pd, which is twice as much as that of commercial Pd black (196.7 mA $mg^{-1}$). The corresponding peak potential of the Pd arrow-headed tripods is located at *ca.* 0.24 V, ~90 mV more negative than that for the commercial Pd black catalyst. Notably, the forward peak current for formic acid electro-oxidation on the electrochemically cleaned Pd arrow-headed tripods is further increased to 493.0 mA $mg^{-1}$ Pd, which is ~250% that of commercial Pd black. The electro-activity of the as-prepared or electrochemically cleaned Pd arrow-headed tripods is also higher than those for the nanodendrites or irregular Pd nanoparticles formed when $Na_2PdCl_4$ or $PdCl_2$ was applied in the preparation (Fig. S4, ESI†). The electrochemically active surface area (ECSA) of the as-prepared Pd arrow-headed tripods measured by CO stripping (details are described in the ESI†) is *ca.* 20 $m^2$ $g^{-1}$ which is *ca.* 1.6 times that of the commercial Pd black (*ca.* 12 $m^2$ $g^{-1}$), revealing that the as-prepared Pd arrow-headed tripods possess a high surface area despite their relatively large overall particle size. In addition to the mass activity, the as-prepared Pd arrow-headed tripods also exhibit a specific activity of 2.0 mA $cm^{-2}$ which is 1.2 times that of the commercial Pd black (1.6 mA $cm^{-2}$), indicating the improved intrinsic activity of the as-prepared Pd arrow-headed tripods. Thus, the improved mass activity of the as-prepared Pd arrow-headed tripods is probably related to the unique morphology of the arrow-headed tripod where high density of low-coordinate atomic steps and kinks (involving high-energy facets), as well as a high surface-area-to-volume ratio exist on the concave regions of the branched arms.[5,8,12] The further increase of the electro-activity on the electrochemically cleaned Pd arrow-headed tripods is probably related to the exposure of more Pd active sites after the removal of the surfactant PVP.

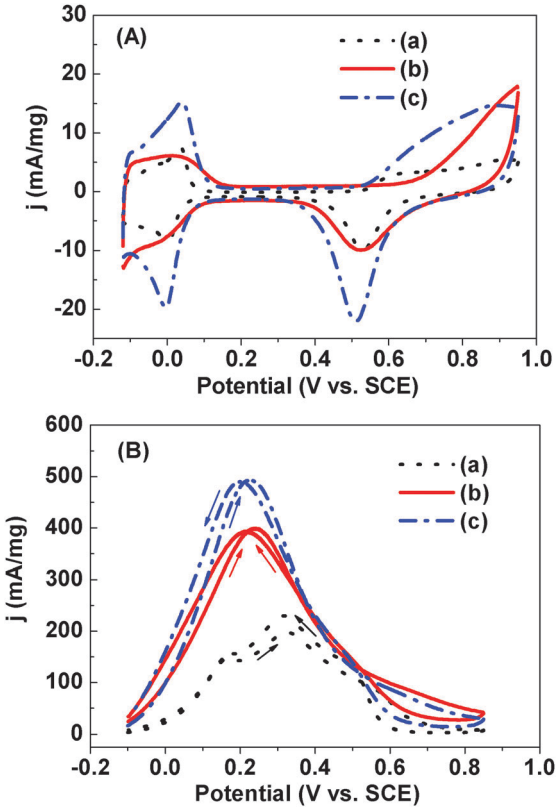


Fig. 4 Cyclic voltammograms at a scan rate of 50 mV $s^{-1}$ in (A) a 0.5 M $H_2SO_4$ solution and (B) a 0.5 M HCOOH + 0.5 M $H_2SO_4$ solution measured on a rotating glass carbon electrode modified with (a) commercial Pd black (BASF), (b) Pd arrow-headed tripods as-prepared, and (c) Pd arrow-headed tripods after being electrochemically cleaned.

In conclusion, single crystalline Pd arrow-headed tripods were successfully prepared using a simple one-pot strategy and their application in formic acid electro-oxidation was studied. The Pd arrow-headed tripods with higher density of atomic steps and kinks appear to exhibit much better electro-activity than the commercial Pd black, which could be promising as an anodic catalyst for DFAFCs.

This work was supported by the National Natural Science Foundation of China (21343003), the Shanghai Science and Technology Committee (12ZR1401400) and the Ministry of Education (the Scientific Research Foundation for the Returned Overseas Chinese Scholars).

## Notes and references

1 S. Mostafa, F. Behafarid, J. R. Croy, L. K. Ono, L. Li, J. C. Yang, A. I. Frenkel and B. R. Cuenya, *J. Am. Chem. Soc.*, 2010, **132**, 15714.
2 M. E. E. Davis and R. J. J. Davis, *Fundamentals of Chemical Reaction Engineering*, McGraw-Hill Higher Education, New York, 2003.
3 R. Narayanan and M. A. El-Sayed, *Nano Lett.*, 2004, **4**, 1343.
4 C. Burda, X. B. Chen, R. Narayanan and M. A. El-Sayed, *Chem. Rev.*, 2005, **105**, 1025.
5 H. Zhang, M. S. Jin and Y. N. Xia, *Angew. Chem., Int. Ed.*, 2012, **51**, 7656.
6 S. H. Chen, Z. L. Wang, J. Ballato, S. H. Foulger and D. L. Carroll, *J. Am. Chem. Soc.*, 2003, **125**, 16186.
7 J. Watt, N. Young, S. Haigh, A. Kirkland and R. D. Tilley, *Adv. Mater.*, 2009, **21**, 2288.
8 B. Lim and Y. N. Xia, *Angew. Chem., Int. Ed.*, 2011, **50**, 76.
9 Y. Dai, X. L. Mu, Y. M. Tan, K. Q. Lin, Z. L. Yang, N. F. Zheng and G. Fu, *J. Am. Chem. Soc.*, 2012, **134**, 7073.
10 Y. T. Chu, K. Chanda, P. H. Lin and M. H. Huang, *Langmuir*, 2012, **28**, 11258.
11 J. Watt, S. Cheong and R. D. Tilley, *Nano Today*, 2013, **8**, 198.
12 H. Zhu, G. Li, X. C. Lv, Y. X. Zhao, T. Huang, H. F. Liu and J. L. Li, *RSC Adv.*, 2014, **4**, 6535.
13 G. A. Somorjai, *Introduction to Surface Chemistry and Catalysis*, Wiley, New York, 1994.
14 P. Waszczuk, T. M. Barnard, C. Rice, R. I. Masel and A. Wieckowski, *Electrochem. Commun.*, 2002, **4**, 599.
15 H. Z. Yang, Y. G. Tang and S. Z. Zou, *Electrochem. Commun.*, 2014, **38**, 134.
16 V. Germain, J. Li, D. Ingert, Z. L. Wang and M. P. Pileni, *J. Phys. Chem. B*, 2003, **107**, 8717.
17 C. Lofton and W. Sigmund, *Adv. Funct. Mater.*, 2005, **15**, 1197.
18 B. K. Lim, M. J. Jiang, J. Tao, P. H. C. Camargo, Y. M. Zhu and Y. N. Xia, *Adv. Funct. Mater.*, 2009, **19**, 189.
19 Y. J. Kang, J. B. Pyo, X. C. Ye, R. E. Diaz, T. R. Gordon, E. A. Stach and C. B. Murray, *ACS Nano*, 2012, **7**, 645.

 